

Acceleration of Passive Tracers in Compressible Turbulent Flow

Yantao Yang, Jianchun Wang, Yipeng Shi,* Zuoli Xiao, X. T. He, and Shiyi Chen†

State Key Laboratory for Turbulence and Complex Systems, Center for Applied Physics and Technology, and Key Laboratory of High Energy Density Physics Simulation (Ministry of Education), College of Engineering, Peking University, Beijing, 100871, China

(Received 6 September 2012; published 7 February 2013)

In compressible turbulence at high Reynolds and Mach numbers, shocklets emerge as a new type of flow structure in addition to intense vortices as in incompressible turbulence. Using numerical simulation of compressible homogeneous isotropic turbulence, we conduct a Lagrangian study to explore the effects of shocklets on the dynamics of passive tracers. We show that shocklets cause very strong intermittency and short correlation time of tracer acceleration. The probability density function of acceleration magnitude exhibits a -2.5 power-law scaling in the high compression region. Through a heuristic model, we demonstrate that this scaling is directly related to the statistical behavior of strong negative velocity divergence, i.e., the local compression. Tracers experience intense acceleration near shocklets, and most of them are decelerated, usually with large curvatures in their trajectories.

DOI: [10.1103/PhysRevLett.110.064503](https://doi.org/10.1103/PhysRevLett.110.064503)

PACS numbers: 47.27.E-, 47.40.-x

Compressible fluid turbulence has proven to be a key phenomenon in many natural environments and engineering flows, including star formation from interstellar gas [1], inertial confinement fusion [2], and hypersonic aircraft. One interesting problem is the motion of particles in those flows, which is crucial to understanding transport and mixing in turbulence [3–5]. The Lagrangian investigation has attracted increasing interest, and it has significantly advanced our knowledge of turbulence. For incompressible flow, it is now possible to track large numbers of particles simultaneously; see Ref. [6] and references therein. Experimental and numerical results have revealed that particle acceleration exhibits strong intermittency that is primarily caused by intense vortex filaments [7–9], and up to 40 times the root mean square (rms) value has been observed [10]. The probability density function (PDF) of acceleration magnitude obeys a log-normal distribution [11].

However, it is very difficult to track particles in experiments with compressible turbulence. Numerical simulation serves as the major tool for Lagrangian study. Some efforts have been made to develop the Lagrangian numerical simulation [12–14] and to explore the mass distribution in isothermal flow [15,16] and the alignment dynamics for isentropic compressible magnetohydrodynamics [17]. Recently, the passive tracer has been used in a compressible turbulence simulation to investigate pair dispersion and mixing in the cosmic intracluster medium [18]. The Lagrangian investigation of passive tracers has also been used to explore the difference between solenoidal and compressive forcing for an isothermal ideal gas flow [19]. In this Letter, we focus on the effects of shocklets on the dynamics of passive tracers, particularly their acceleration, using three-dimensional compressible viscous turbulent flow.

We simulate three-dimensional compressible turbulence in a periodic box of width 2π . A novel hybrid numerical method with a resolution of 512^3 is used [20]. After the flow reaches a statistically steady state, a million passive tracers are seeded uniformly into the flow domain. The dynamic equations for a passive tracer in dimensionless form are given by

$$\dot{\mathbf{x}}(t) = \mathbf{u}(\mathbf{x}, t), \quad (1)$$

$$\dot{\mathbf{u}} = \mathbf{a} = -\frac{1}{\rho\gamma M^2}\nabla p + \frac{1}{\rho\text{Re}}\nabla\cdot\boldsymbol{\sigma} + \mathcal{F}, \quad (2)$$

where \mathbf{x} , \mathbf{u} , and \mathbf{a} denote the location, velocity, and acceleration of the tracer, respectively; ρ is local density; p is pressure; $\boldsymbol{\sigma}$ is the viscous stress tensor; and γ is the ratio of specific heat at constant pressure to that at constant volume. A dot stands for the Lagrangian or material derivative. The Mach number $M = U/c$ is defined as the ratio of velocity to the speed of sound. The Reynolds number Re is equal to $\rho UL/\mu$ with L being the length and μ the dynamic viscosity. The three terms on the right-hand side of (2) represent the accelerations due to the pressure gradient, viscous stress, and external driving force, respectively.

In order to track the tracer, Eq. (1) is solved by using the second-order Runge-Kutta method. The physical quantities of the tracer are calculated by a trilinear interpolation to avoid unphysical oscillations near shocklets. Recent studies suggest that the Kolmogorov phenomenology can be extended to compressible turbulence [21–23]. Thus we may define the viscous scale $\eta = (\nu^3/\epsilon)^{1/4}$ and the Kolmogorov time $\tau_\eta = (\nu/\epsilon)^{1/2}$, where ν is the kinematic viscosity and ϵ is the energy-dissipation rate per unit mass. To accurately track tracers, we set the grid size to be $dx \approx 0.96\eta$ and update locations every $\tau_\eta/100$. The total

integration time is about $10T^E$, where T^E is the large eddy turnover time. We compute the Lagrangian statistics during the last $8T^E$ with a sampling interval of $\tau_\eta/10$. The resulting turbulent Mach number $M_T = u_{\text{rms}}/\bar{c} \approx 1.03$. Hereafter, the subscript “rms” denotes the root mean square value, and the overline represents the average over all particles and time. The Reynolds number based on the Taylor microscale Re_λ is about 153. The Lagrangian integral time scale T^L , which is defined by the integral of the velocity autocorrelation, is about 1.07. For comparison, T^E is about 1.1 and τ_η about 0.063.

We use the dilatation $\theta = \nabla \cdot \mathbf{u}$ to identify the flow region with different local compression. A large negative θ indicates strong compression. In order to isolate the compression effect, we decompose the entire flow domain into three regions: (a) the compression region with $\theta < -\theta_{\text{rms}}^n$, (b) the smooth region with $-\theta_{\text{rms}}^n < \theta < \theta_{\text{rms}}^p$, and (c) the expansion region with $\theta > \theta_{\text{rms}}^p$. Here θ_{rms}^n and θ_{rms}^p are the rms values computed from negative and positive θ of the Eulerian field, respectively.

A major difference between compressible and incompressible flow is the appearance of shocklets [20,24]. In Fig. 1(a), we show instantaneous volume renderings of two different types of flow structures, i.e., sheetlike shocklets and tubelike vortices. In the same figure, we also place several typical particle trajectories near those flow structures. An immediate observation is that tracers change their

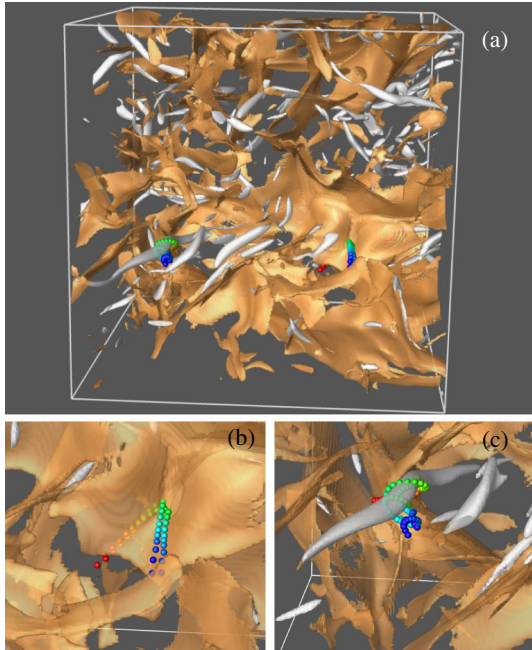


FIG. 1 (color online). (a) Instantaneous rendering of shocklets (dark brown sheetlike surface) and vortices (light gray tubelike surface), with typical tracer trajectories. (b) Tracers changing direction near a shocklet. (c) Tracers rotating around a vortex. Trajectories start from the near (blue) ends and last for a time period of $10\tau_\eta$.

directions abruptly when they cross the shocklets, as shown in Fig. 1(b). Away from the shocklets, tracers may rotate around the intense vortices, as shown in Fig. 1(c). Thus, for compressible turbulence the shocklet is a new source of extreme acceleration other than intense vortices.

The two different types of tracer motion caused by shocklets and vortices together determine the time dynamics of acceleration. Figure 2 shows the Lagrangian autocorrelations of acceleration magnitude a and three Cartesian components a_i with $i = 1, 2, 3$, which are defined as $R = \overline{a'(t)a'(t+\tau)}/a_{\text{rms}}^2$. Here, $a'(t) = a(t) - \bar{a}$. The curves of the incompressible flow from Ref. [11] are also shown for comparison. Autocorrelations in the compressible case decay much faster than those in the incompressible case, which may be attributed to the shocklets.

Furthermore, we have calculated the autocorrelation coefficients near different flow structures. For shocklets, $R^s = \langle a'(0)a'(\tau) \rangle / (\sqrt{\langle a'(0)^2 \rangle} \sqrt{\langle a'(\tau)^2 \rangle})$. Here, $\langle \cdot \rangle$ represents the ensemble average over all possible time intervals $0 < \tau < \tau_\eta$, during which θ has a local minimum that is smaller than $-\theta_{\text{rms}}^n$. R^v is calculated with the same formula for all time intervals $0 < \tau < 5\tau_\eta$, during which tracers stay in the smooth vortical region with $-\theta_{\text{rms}}^n < \theta < \theta_{\text{rms}}^p$. Acceleration decorrelates much faster near shocklets than near vortices. When tracers move through shocklets, they experience extremely high acceleration during a short period, as shown in inset (a) in Fig. 3. The peak value is much bigger than the average over the entire domain. Naturally, the autocorrelation coefficients will quickly decay when τ is larger than the width of the acceleration burst. Figure 3 indicates that R^s of magnitude drops to around 0.5 at $\tau = 0.1\tau_\eta$. R^s of magnitude decays slightly faster than those of the components, since shocklets induce only large acceleration normal to the shock surface and have little effect on the tangential component. The curves in the vortical region are very similar to those of incompressible flow reported in Ref. [11]. R^v of components

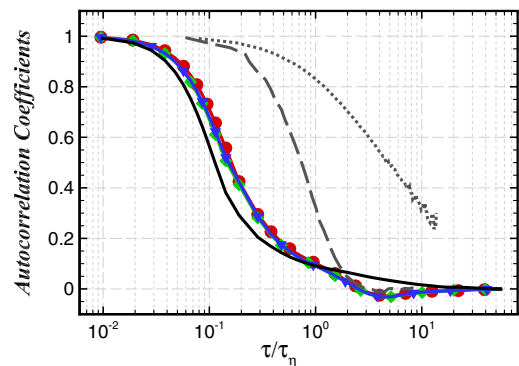


FIG. 2 (color online). The autocorrelation coefficients of acceleration magnitude a (black line) and components a_i (lines with symbols), compared to the autocorrelations of magnitude (dotted line) and one component (dashed line) of an incompressible flow (reproduced from Ref. [11]).

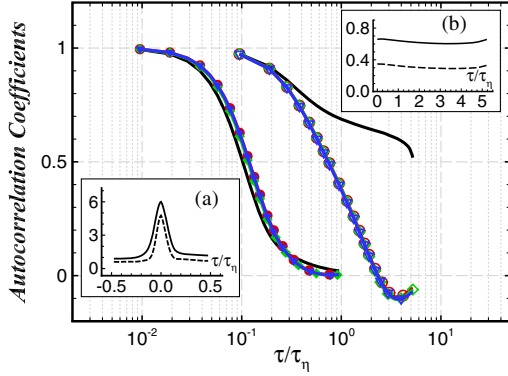


FIG. 3 (color online). Autocorrelation coefficients R^s (left bunch) and R^v (right bunch), with the same line style as Fig. 2. The insets show $\langle a(\tau) \rangle / \bar{a}$ and $\sqrt{\langle a'(\tau)^2 \rangle} / a_{rms}$ with solid and dashed lines, respectively. (a) Near shocklets and (b) trapped by vortices.

cross zero at around $2.3\tau_\eta$. The ensemble average and rms of a remain nearly constant when tracers are trapped by vortices, as shown in inset (b) in Fig. 3.

In Fig. 4, we show the total PDF of acceleration magnitude and the PDFs in the three different regions. For large a , the total PDF curve overlaps with that of the compression region, which implies that the extreme acceleration events are all detected near the shocklets. For small a , the smooth and expansion regions contribute to the major portion of the total PDF. The expansion region, which is often located closely downstream from the shocklets, does not induce very large acceleration. As shown in inset (a) in Fig. 4, the PDF curve of the smooth region matches the log-normal distribution with a variance of 1, as proposed for incompressible turbulence by Refs. [11,25]. This implies that, in the low-dilatation region of compressible turbulence, the tracer acceleration behaves similarly to that in incompressible turbulence.

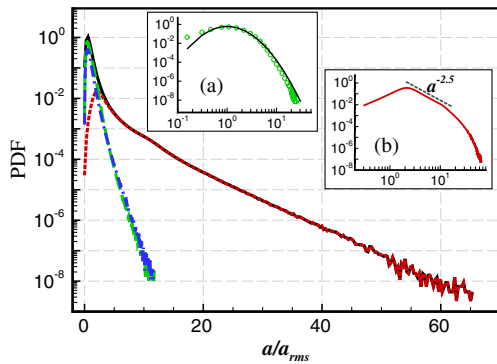


FIG. 4 (color online). Log-linear plots of the PDFs of acceleration magnitude a in three flow regions, normalized by the total number of data points. Black solid line: all tracers; red dotted line: the compression region; green dashed line: the smooth region; and blue dash-dotted line: the expansion region. Inset (a), Log-normal distribution in the smooth region; and inset (b), -2.5 power-law distribution in the compression region.

The curve of the compression region develops a $a^{-2.5}$ power law in the PDF tail; see inset (b) in Fig. 4. It has been found that in the shocklet region, the θ PDF also follows the -2.5 power law [26]. Figure 5 shows the joint PDF of a and θ , $P(a, \theta)$. A distinct ridge exists in the negative θ region. We also plotted the PDF quotient $Q = \frac{P(a, \theta)}{P(a)P(\theta)}$ [27], which measures the correlation between a and θ . $Q > 1$ ($Q < 1$) represents positive (negative) correlation. The contours immediately suggest that a large acceleration is very likely accompanied by a large magnitude of θ , which usually happens near shocklets.

The strong correlation between the large acceleration and strong compression may be explained as follows. Let us denote the three principle axes of the strain-rate tensor by \mathbf{e}_i with $i = 1, 2, 3$, which are associated with the eigenvalues sorted in descending order. Near strong shocklets, the compression occurs mainly in the \mathbf{e}_3 direction. Without losing generality, we set \mathbf{e}_3 to point from upstream of the shocklet to downstream. Then, the velocity divergence can be approximated by $\theta \approx (w_2 - w_1)/dl$, where w_1 and w_2 are the velocity components in the \mathbf{e}_3 direction upstream and downstream of shocklet, respectively, and dl is the shock thickness. It is reasonable to assume that the time scale of shocklet evolution is much longer than the time it takes a tracer to cross the shock region. Therefore, tracer acceleration can be calculated approximately as $a \approx |w_2 - w_1|/dt$, where dt is the time for a tracer to travel through a shocklet. Immediately, one has $a \approx |\theta|dl/dt = |\theta|u_n$, where u_n can be treated as the normal velocity with which the tracer moves through a shocklet.

Using the above model, we can compute the PDF of a from that of θ . In shocklets region the θ PDF has power-law scaling at $\theta < 0$, i.e., $f_{|\theta|} \sim |\theta|^\zeta$ with $\zeta \approx -2.5$ [26]. Our numerical results have indicated that u_n is statistically independent of θ and has a quasi-Gaussian distribution, which we denote as f_{u_n} . Then, by the algebra of random variables, we have

$$f_a(a) \sim \int f_{u_n}(u_n)(a/u_n)^\zeta u_n^{-1} du_n = Ca^\zeta. \quad (3)$$

Thus, the a PDF must have the same power-law scaling as the θ PDF, which is exactly what we found in our simulation.

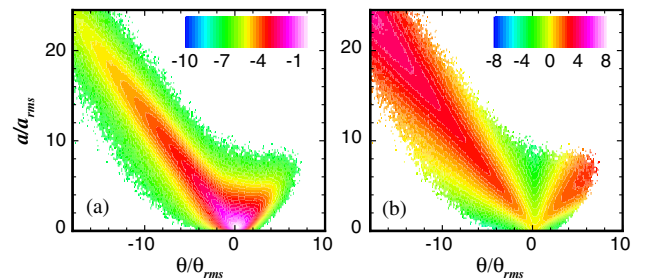


FIG. 5 (color online). (a) Logarithm of the joint PDF $P(a, \theta)$. (b) Logarithm of the PDF quotient $Q(a, \theta)$.

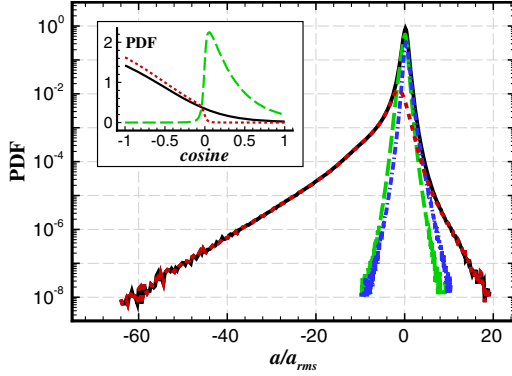


FIG. 6 (color online). PDFs of a_L in different regions with the same line styles as in Fig. 4, normalized by the total number of data points. Inset: PDFs of $\cos\alpha$ in the compression region, normalized separately. Black solid line: sampled over all tracers; red dotted line: decelerated tracers with $a_L < 0$; and green dashed line: accelerated tracers with $a_L > 0$.

To further understand the tracer motion near shocklets, we decompose the acceleration into a longitudinal component $a_L = \mathbf{a} \cdot \mathbf{u}/|\mathbf{u}|$ and a transverse component $\mathbf{a}_T = \mathbf{a} - a_L \mathbf{u}/|\mathbf{u}|$. Evidently, a_L determines the time-changing rate of the velocity magnitude. \mathbf{a}_T is directly linked to the curvature of tracer trajectory, which will be discussed later. The PDFs of a_L are plotted in Fig. 6. The curve of the smooth region is symmetric about $a_L = 0$, which is the same as in our incompressible results (not shown here). The PDF of the expansion region shows slight asymmetry, and the peak is located at a very small positive value. The PDF of the compression region has very strong asymmetry, and the left tail is much longer than the right one. In the compression region, the negative pressure gradient $-\nabla p$ is basically perpendicular to the shocklet surface pointing upstream and in the direction of acceleration according to (2). We investigated the cosine of the angle α between the velocity \mathbf{u} and negative pressure gradient $-\nabla p$. The PDF of $\cos\alpha$ in the compression region is plotted in the inset in Fig. 6. It has a peak at $\cos\alpha = -1$ (solid line), which means that tracers are most likely to hit shocklets vertically from upstream. For most decelerated tracers, $\cos\alpha < 0$ (dotted line), and they move against the shocklets. Some tracers are accelerated near shocklets with $\cos\alpha > 0$ (dashed line). Basically, these tracers are overtaken by shocklets. Numerical results show that the ratio of the numbers of decelerated tracers to accelerated ones is 7:1 for the present case.

We now focus on the curvature of tracer trajectory, which is directly related to the transverse acceleration \mathbf{a}_T by $\kappa \equiv |\mathbf{a}_T|/u^2$ [27]. Near shocklets, the total acceleration is very likely perpendicular to the shock surface. When a tracer moves obliquely through such structures, it undergoes strong transverse acceleration, and its trajectory may have a very large curvature in these regions. The PDFs of κ in different regions are plotted in Fig. 7. At the present

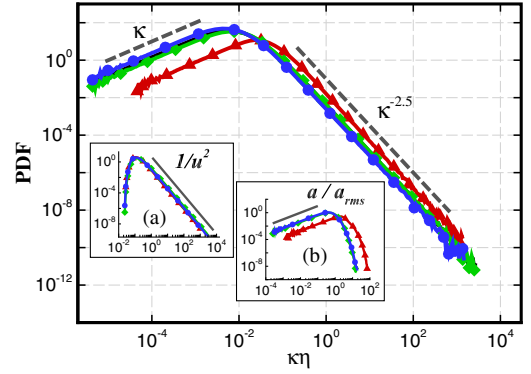


FIG. 7 (color online). Log-log plot of PDF distribution of normalized curvature $\kappa\eta$ of the whole field (black solid line), the compression region (red triangle), the smooth region (green diamond), and the expansion region (blue circle). Inset (a): the $-5/2$ scaling of $1/u^2$ as $u^2 \rightarrow 0$. Inset (b): the linear scaling of a_T as $a_T \rightarrow 0$.

Reynolds and Mach numbers, the peak of total PDF is located at $\kappa\eta \approx 5.8 \times 10^{-3}$, which is very close to that of incompressible flow [27]. The two tails of all PDF curves exhibit the same power laws as the incompressible case [27]. This is to be expected, because the extremely small and large curvatures are associated with the statistical behavior of a_T as $a_T \rightarrow 0$ and $1/u^2$ as $u \rightarrow 0$. The insets show that the $1/u^2$ PDF is almost the same for the three different regions, and the compressibility only shifts the PDF of a_T toward a larger value. Consequently, the κ PDF of the compression region also shifts toward a larger curvature value. The peak of PDF in the compression region is located at $\kappa\eta \approx 2.4 \times 10^{-2}$. We believe that, for a higher Mach number, this PDF curve would move even farther into the larger curvature region.

In conclusion, we present several significant effects of shocklets on the dynamics of passive tracers in compressible turbulence. Shocklets induce very large acceleration in a very short time period and therefore quickly decorrelate the acceleration magnitude and components. The PDF of acceleration magnitude in the compression region obeys a -2.5 power-law scaling, which is directly related to the PDF of negative θ . Most tracers move through shocklets from upstream, during which they experience obvious deceleration and strong lateral acceleration due to the large adverse pressure gradient. Meanwhile, large curvatures appear in their trajectories. It is also found that a small portion of tracers may be accelerated as they are overtaken by shocklets. Even though the present study is based on one single set of parameters, we infer that the main conclusions are still qualitatively applicable for higher Mach and Reynolds numbers.

The authors appreciate the valuable comments of the anonymous referees. This work was supported partially by the National Natural Science Foundation of China (NSFC Grants No. 10902002, No. 10921202, and No. 91130001)

and the National Science and Technology Ministry under a subproject of the 973 program (Grant No. 2009CB724101). Y. Y. acknowledges partial support by NSFC Grant No. 11274026 and China Postdoctoral Foundation Grant No. 2011M500194. The simulations were done on the TH-1A supercomputer at Tianjin, China.

*ypshi@coe.pku.edu.cn

†syc@pku.edu.cn

- [1] M.-M. Mac Low and R. S. Klessen, *Rev. Mod. Phys.* **76**, 125 (2004).
- [2] V. A. Thomas and R. J. Keres, *Phys. Rev. Lett.* **109**, 075004 (2012).
- [3] S. Pope, *Annu. Rev. Fluid Mech.* **26**, 23 (1994).
- [4] B. I. Shraiman and E. D. Siggia, *Nature (London)* **405**, 639 (2000).
- [5] P. Yeung, *Annu. Rev. Fluid Mech.* **34**, 115 (2002).
- [6] F. Toschi and E. Bodenschatz, *Annu. Rev. Fluid Mech.* **41**, 375 (2009).
- [7] L. Biferale, G. Boffetta, A. Celani, A. Lanotte, and F. Toschi, *Phys. Fluids* **17**, 021701 (2005).
- [8] F. Toschi, L. Biferale, G. Boffetta, A. Celani, B. Devenish, and A. Lanotte, *J. Turbul.* **6**, N15 (2005).
- [9] A. Reynolds, N. Mordant, A. Crawford, and E. Bodenschatz, *New J. Phys.* **7**, 58 (2005).
- [10] A. La Porta, G. A. Voth, A. M. Crawford, J. Alexander, and E. Bodenschatz, *Nature (London)* **409**, 1017 (2001).
- [11] N. Mordant, A. M. Crawford, and E. Bodenschatz, *Phys. Rev. Lett.* **93**, 214501 (2004).
- [12] H. Schamel, *Phys. Rep.* **392**, 279 (2004).
- [13] S. Kitsionas, C. Federrath, R. Klessen, W. Schmidt, D. Price, L. Dursi, M. Gritschneider, S. Walch, R. Piontek, J. Kim, A. Jappsen, P. Ciecielag, and M. Mac Low, *Astron. Astrophys.* **508**, 541 (2009).
- [14] V. Springel, *Annu. Rev. Astron. Astrophys.* **48**, 391 (2010).
- [15] C. Beetz, C. Schwarz, J. Dreher, and R. Grauer, *Phys. Lett. A* **372**, 3037 (2008).
- [16] C. Schwarz, C. Beetz, J. Dreher, and R. Grauer, *Phys. Lett. A* **374**, 1039 (2010).
- [17] J. Gibbon and D. Holm, *New J. Phys.* **9**, 292 (2007).
- [18] F. Vazza, C. Gheller, and G. Brunetti, *Astron. Astrophys.* **513**, A32 (2010).
- [19] L. Konstandin, C. Federrath, R. Klessen, and W. Schmidt, *J. Fluid Mech.* **692**, 183 (2011).
- [20] J. Wang, L. P. Wang, Z. Xiao, Y. Shi, and S. Chen, *J. Comput. Phys.* **229**, 5257 (2010).
- [21] G. Falkovich, I. Fouxon, and Y. Oz, *J. Fluid Mech.* **644**, 465 (2010).
- [22] H. Aluie, *Phys. Rev. Lett.* **106**, 174502 (2011).
- [23] H. Aluie, S. Li, and H. Li, *Astrophys. J. Lett.* **751**, L29 (2012).
- [24] R. Samtaney, D. Pullin, and B. Kosović, *Phys. Fluids* **13**, 1415 (2001).
- [25] C. Beck, *Phys. Rev. Lett.* **98**, 064502 (2007).
- [26] J. Wang, Y. Shi, L. P. Wang, Z. Xiao, X. T. He, and S. Chen, *Phys. Rev. Lett.* **108**, 214505 (2012).
- [27] H. Xu, N. T. Ouellette, and E. Bodenschatz, *Phys. Rev. Lett.* **98**, 050201 (2007).